Variation of cloud horizontal sizes and cloud fraction over Europe 1985–2018 in high-resolution satellite data

Linke, O.[1,✉], **Quaas, J.**[1]

[1] *Leipzig Institute for Meteorology, Leipzig University*
✉*e-mail: olivia.linke@uni-leipzig.de*

Summary: Aerosol-cloud interactions are a major uncertainty in estimating the anthropogenic climate change. Adjustments of cloud properties to an aerosol perturbation concern among others the cloud fraction, and have been emphasised as particularly complex.

Cloud adjustments can generate important responses on the distribution of cloud horizontal sizes. We derive the cloud-size distribution as observational constraint for the cloud-fraction response from high-resolution Landsat satellite data. The goal is to carry out long-term trends in cloud sizes and cloud fraction over Europe during 1985–2018 to investigate the impact of major aerosol reductions during that time. Landsat data with a high spatial resolution of 30 m was preprocessed via the web-based platform Google Earth Engine to evade the obstacle of high computational effort and time to handle the comprehensive data archive.

The observed multidecadal trends indicate a widespread increase in cloud fraction during 1985–2018. This corresponds to a decrease in the number of small clouds of several 10–100 m cloud length, whereas larger clouds (1 km and more), which contribute more to the cloud fraction, became more numerous. We confirm this by showing a large-scale decrease of the power-law exponent describing the relative abundance of small and large clouds in the cloud-size distribution. Even though we can interpret the observed changes in cloud properties as significant trends, we do not explicitly identify a clear aerosol signal. Untangling the pure aerosol effect from other confounding factors (e.g., the local meteorology) is therefore left as an outlook for subsequent studies.

Zusammenfassung: Aerosol-Wolken-Wechselwirkungen stellen eine große Unsicherheit in der Quantifizierung des anthropogenen Klimawandels dar. Die sekundären Anpassungen von Wolken an eine Veränderung atmosphärischer Aerosolkonzentrationen betreffen beispielsweise den Wolken-Bedeckungsgrad und sind besonders komplex. Wolkenanpassungen können sich in der Veränderung der Wolkengrößen-Verteilung widerspiegeln. Wir präsentieren eine Methode, um mittels Beobachtungen der Wolkengrößen-Verteilung zeitliche Veränderungen in Aerosol-Wolken-Wechselwirkungen nachzuweisen.

Wolkengrößen-Verteilung und Wolkenbedeckungsgrad wurden mittels hochauflösender Satellitendaten der Landsat-Serie berechnet. Das Ziel ist es, langjährige Trends im Wolkenbedeckungsgrad über Europa im Zeitraum 1985–2018 herzuleiten und ggf. den Einfluss stark rückläufiger Aerosolkonzentrationen während dieser Zeit zu identifizieren. Landsat-Daten haben eine räumliche Auflösung von bis zu 30 Metern. Um die damit verbundenen großen Datenmengen prozessieren zu können, nutzen wir die Web-basierte Plattform Google Earth Engine.

Unsere langjährigen Trends zeigen eine großskaligen Zunahme im Wolkenbedeckungsgrad zwischen 1985 und 2018. Dies ist zurückzuführen auf einen relativen Rückgang in der Anzahl kleinerer Wolken (einige 10 bis 100 Meter Länge), während größere Wolken (mehrere Kilometer), welche mehr zum Bedeckungsgrad beitragen, häufiger wurden. Dies zeigt sich im negativen Trend des Power-Law-Exponenten der Wolkengrößen-Verteilung, welcher die relative Anzahl kleiner und großer Wolken beschreibt. Auch wenn sich diese Beobachtungen als signifikante Trends herausstellen, identifizieren wir darin kein klares Aerosol-Signal. Die Isolierung des puren Aerosoleffekts von anderen beeinflussenden Faktoren, wie der lokalen Meteorologie, bietet einen Ansatzpunkt für aufbauende Studien.

1 Introduction

Clouds are important regulators of the Earth's energy balance due to their strong impact on fluxes of incoming shortwave radiation (SWR), and outgoing longwave radiation (LWR) that is emitted by the Earth. Since clouds interact with both SWR and LWR, small changes in cloud properties may have important implications on the Earth radiation budget (Boucher et al., 2013; Cubasch et al., 2013).

Several human impacts have the potential to alter cloud characteristics and abundance. Among these are changes in anthropogenic aerosol emissions. Aerosol particles serve as cloud condensation nuclei (CCN) in almost all liquid-water nucleation processes, thereby mediating cloud radiative properties (Lohmann and Feichter, 2005). Aerosol-cloud interactions (ACIs) have an important impact on the top-of-the-atmosphere (TOA) radiative effect, but still contribute largely to the uncertainty in quantifying anthropogenic climate change (Boucher et al., 2013).

It is commonly known that changes in the amount of aerosol particles can impact the number concentration of cloud droplets which affects the cloud albedo (Twomey, 1974). However, there are conflicting results on the sign of the RF arising from cloud adjustments, making it particularly challenging to understand the full impact of ACIs (e.g., Jiang et al., 2006; Xue et al., 2008; Small et al., 2009).

Those adjustments concern the aerosol effect on cloud properties like the cloud lifetime, liquid water path (LWP), and the cloud fraction (CF): It is likely that an increased state of pollution corresponds to more numerous, but smaller droplets at initially unchanged LWP (Twomey, 1974). Some clouds (e.g., warm boundary layer clouds) can adjust to the smaller droplets through the suppression of precipitation. This process is widely known as "lifetime effect" as it potentially extends the residence time of cloud condensate (Albrecht, 1989).

However, several model-based and observational studies reinforce that a non-linear relationship exists within the cloud adjustments (e.g., Jiang et al., 2006; Xue et al., 2008; Small et al., 2009). Other processes can feed back on cloud radiative properties as a consequence of initially changed CCN. Those processes include possible evaporation feedbacks that can reduced cloudiness as a consequence of an increase in aerosol concentrations. The feedbacks thereby counteract the lifetime effect and have the potential to offset a significant fraction of the Twomey effect (Gryspeerdt et al., 2018).

We speculate on the role of cloud horizontal sizes and propose that small and large clouds likely show different responses to changing aerosol concentrations: The addition

of aerosols may increase the size of large clouds as they are less susceptible to evaporation drying. On the other hand, if small, non-precipitating cumulus clouds experience an aerosol perturbation, they can respond in a manner incongruent with the lifetime effect, due to their higher surface-to-volume ratio, which feeds back positively on the cloud size (Jiang and Feingold, 2006; Xue and Feingold, 2006; Small et al., 2009).

Based upon this, we enforce the hypothesis that through a changing aerosol concentration the cloud-size distribution (CSD) shifts as response to either lifetime and/or evaporation feedbacks. This potentially provides an observational constraint for the aerosol effects on cloud lifetime and CF which are often assumed to be correlated (Jiang et al., 2006).

To test this hypothesis, we make use of the large-scale reduction of the aerosol load over Europe during past decades: We estimate the CF response by deriving CSDs from high-resolution Landsat data during the period where aerosol concentrations haven been decreasing. The satellite data was provided and preprocessed by the web-based platform Google Earth Engine (GEE) to manage the vast amount of data. A main attempt of this study was to show the capability of exploiting the Landsat-GEE community for deriving trends in CSD and CF over Europe during 1985–2018.

The leading scientific questions of this work are defined as the following: 1) What cloud changes have occurred during recent decades? 2) Are the trends real or spurious, and if real, can they be attributed to the European aerosol decrease since the late 1980s?

This section is followed by a methodological description of estimating CSDs and CF from satellite data. Results are presented as pan-European and long-term averaged CSD firstly. Secondly, we show interannual trends of CSD and CF over Europe 1985–2018. Finally, results are discussed in terms of potential ACIs over Europe from a reduction in aerosols.

2 Data and methods

The cloud-size distribution n is commonly known to follow a negative sloping power-law relation in terms of the cloud length L (or area):

$$n(L) = \alpha L^{-\beta}. \tag{1}$$

The power-law distribution was previously documented for satellite observations and large eddy simulations, and also applies for global data sets. The latter has been demonstrated by Wood and Field (2011). We follow their method and derive $n(L)$ by adding up the total number of clouds N_i with lengths between (approximately logarithmic) bin boundaries $L_{\mathrm{i}-}$ and $L_{\mathrm{i}+}$, and dividing by the respective bin width and total transect length D_{tot}:

$$n(L) = \frac{N_{\mathrm{i}}}{D_{\mathrm{tot}}(L_{\mathrm{i}+} - L_{\mathrm{i}-})}. \tag{2}$$

For a given cloud field that conforms to a power-law distribution, the cloud fraction can be derived by integrating $Ln(L)$ over L,

$$\mathrm{CF}(L_{\min}, L_{\max}) = \int_{L_{\min}}^{L_{\max}} Ln(L)dL, \tag{3}$$

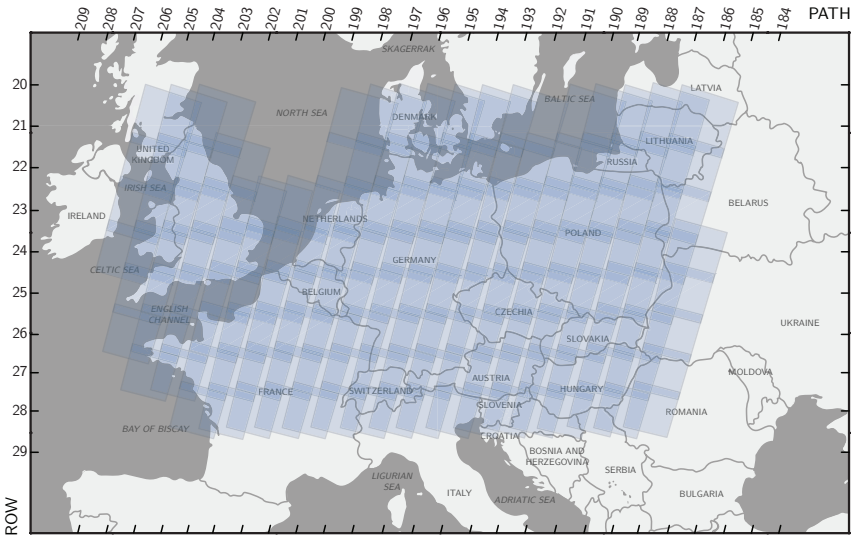

Figure 1: *European research domain showing all Landsat footprints in the region. The spatial attribution follows the path/row WRS-2.*

with $L_{\min}$ and $L_{\max}$ being the smallest and largest detectable scale, respectively.

We use Landsat data from 1985 to 2018 which provides a powerful tool to resolve cloud fields at 30 m horizontal size. To take full advantage of the massive data amount, we use GEE which provides access to high-performance computing resources to process large geospatial data volumes. We use data from the USGS Collection-1 Tier-1 TOA reflectance archive from Landsat 5, 7 and 8. Data from Landsat 7 was included only within 1999–2003 due to a scan-line correction failure which would have affected the results onward from May 2003. Also, the year 2012 is not represented here due to the data gap following the fail of the Landsat-6 mission.

Landsat images are provided within so called footprints/tiles that are spatially classified by satellite path and row according to Worldwide Reference System-2 (WRS-2). Figure 1 gives a map of all tiles considered as our research domain. In total, 143 Landsat tiles were chosen to represent a wide range of the European continent. Each tile has an approximate horizontal size of 200×200 km, and contains around 7000×7000 pixels on average, with 8–11 bands depending on the Landsat mission.

All files within the data collection were passed on to a cloud-masking GEE internal algorithm. From the binary mask, we derive cloud lengths in two different sampling directions (in North-South and West-East alignment) by counting horizontally contiguous cloud pixels between the clear boundaries. A simplified sketch of a cloud-mask example and the sampling in each direction is illustrated in Fig. 2. If the first or last pixel of a given stripe contains a cloud, the corresponding cloud length is initially excluded due to the chance of extending beyond the satellite scene. Each Landsat pixel has a horizontal resolution of 30 m.

We calculate the CSD corresponding to Eq. 2. By ignoring all clouds touching the scene boundary, a size-dependent sampling bias arises since large clouds are more likely being excluded. Wood and Field (2011) address this error by introducing a correction term to Eq. 2. However, applying the correction to the Landsat data was set aside here, since the main interest was to quantify how the CSD changes over the years. Since the image size among all Landsat files does not show distinct variations, the error can be

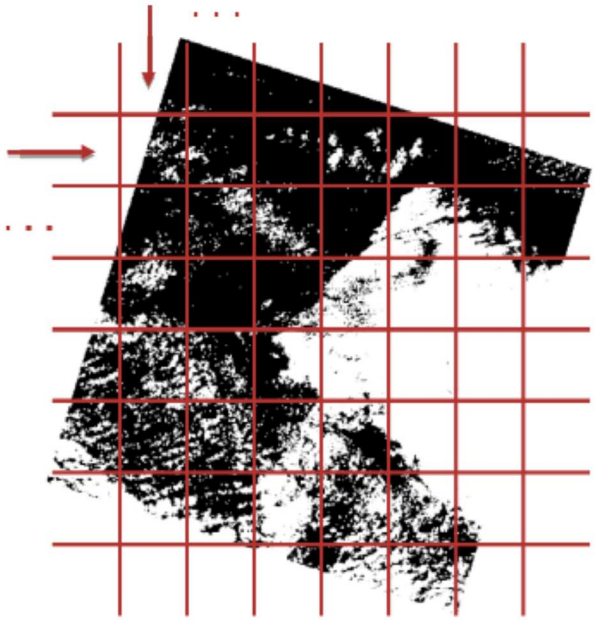

Figure 2: *Sketch of stripe-wise cloud size sampling in the cloud mask (here: white=cloudy pixel, black=non-cloudy pixel). Horizontally contiguous cloud pixel are counted together to add up to a respective cloud length value. The cloud sampling directions are in North-South and West-East alignment. Therefore, each satellite image is scanned twice foe cloud sizes. The resolution of each Landsat image is 30 m.*

considered an equal impact on the results and thereby cancels by looking at temporal changes.

To quantify interannual changes, we fit the observed CSD to Eq. 1 to derive the horizontal exponent β. The exponent is used to determine the pivoting of the CSD over the years (i.e., the change in the frequency of occurrence among the cloud-size classes). Finally, the CF is calculated via Eq. 3, with power-law parameters α and β derived from the power-law fit.

3 Results

We first show the pan-European CSD as a temporal average by grouping together the data for the entire period 1985–2018. Secondly, the data was grouped for each year individually to carry out interannual records of CSD and CF over Europe and potentially detect an aerosol impact.

The single pan-European CSD (Fig. 3) closely matches a power-law relation that spans over three orders of magnitude of cloud size, from 30 m to 30 km. The middle sloping line (black) shows the best regression ($r = 0.996$) between observation and power-law fit. The overall power-law exponent is estimated with $\beta = 1.73$. The blue and green lines represent exponents of $\beta = 1.5$ and $\beta = 1.9$, respectively, to visualise the impact of variable parameters on the CSD. For clouds larger than approximately 30 km length, the distribution deviates from the power law (scale break).

Looking at each Landsat footprint individually, again, all size distributions closely match a power-law relationship (not shown here), with significant individual correlations

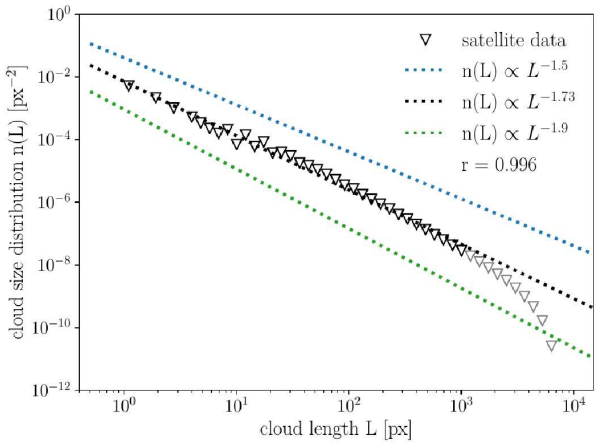

Figure 3: *Observed pan-European CSD, $n(L)$ on the y-axis as temporal average for the time period 1985–2018 (triangles). The exponent β of the power-law is estimated with $\beta = 1.73$. Pearson's correlation coefficient for the regression is $r = 0.996$. 50 logarithmically spaced bins are used to display the distribution. For larger cloud sizes, the distribution deviates from the power-law due to a horizontal scale break (gray triangles).*

between observation and fit. The power-law exponent over Europe spatially varies with $1.63 \leq \beta \leq 1.83$, so that the overall scaling exponent can be quantified as $\beta = 1.73 \pm 0.10$ to account for regional variations.

3.1 Interannual cloud-size distribution trends

Trends in the CSD are derived by grouping the cloud sizes per year, so that each time step accounts for an annual average of the distribution. We do not account for seasonality.

The pan-European trend of the horizontal exponent β during 1985–2018 is represented in Fig. 4. Panel (a) accounts for data averaged over all 143 Landsat tiles of the research domain. The data indicate an overall dropping horizontal exponent over Europe. The overall trend is not monotonic and includes a period of increasing β during 2000–2010.

However, not all time series within individual Landsat footprints give trends that are statistically significant. Panel (b) only includes the data of satellite footprints with robust trends. To ensure the practicability of the linear trend model, we filter among the tiles by excluding all local trends with linear correlation coefficients below 0.4, and a root-mean-square error (RMSE) above the domain-average value.

When including only robust individual time-series, the trend increases from $-1.6 \cdot 10^{-3}$ to $-3.7 \cdot 10^{-3}$ per year with larger correlation ($r = 0.81$), while increasing the error range due to the reduced amount of data (only 21 grid boxes passed the filtering procedure). The corresponding tiles that passed the significance filter are marked in Fig. 5, showing the spatial distribution of trends widespread over Europe. From the 21 tiles that passed the filtering, 17 are found on land and appear in the map as crosses within the respective region.

All statistically significant grid-box trends support a long-term decrease in the power-law exponent. The corresponding regions are mostly found over Germany and in some parts of France, Great Britain, and the Benelux. Considering the entire domain, regions

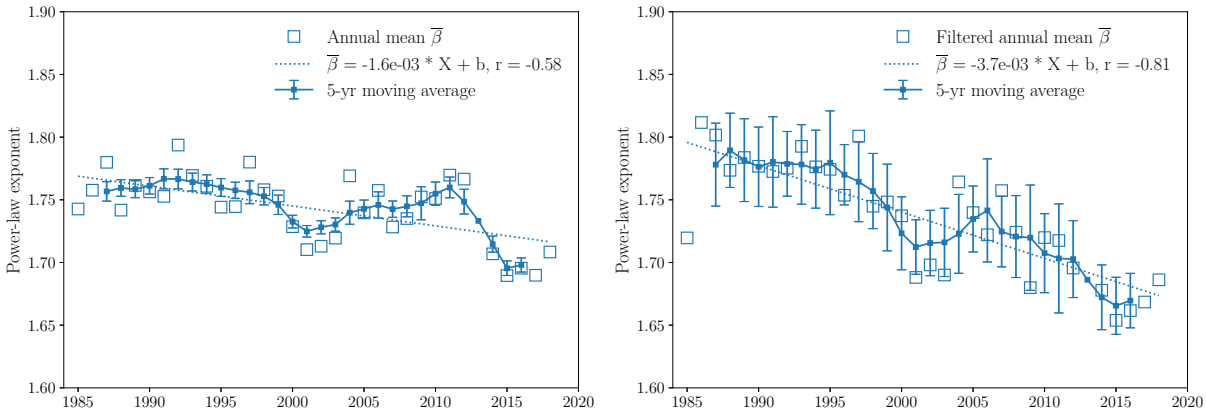

(a) (b)

Figure 4: *Pan-European trends of the power-law scaling exponent $\overline{\beta}$ 1985–2018, (a) without filtering, and (b) after filtering, as raw data (larger empty squares), and low-frequency variability (5-yr moving average time series; filled smaller squares). The filtering in (b) excludes all Landsat footprints with individual correlation coefficients $r < 0.4$, and a RMSE > $\overline{RMSE}$ (domain average), respectively. Error bars are indicated as standard error of mean. A linear regression fit is used to derive the trend in $\overline{\beta}$ 1985–2018.*

with negative trends dominate the geographic pattern.

In summary, there was an overall dropping horizontal scaling exponent describing the CSD over Europe during 1985–2018, with locally significant trends supporting the result. The negative trend corresponds to a large-scale pivoting of the negative power-law slope as result of both a decreased number of small clouds, and an increase in the number of larger cloud fields. The latter was not specifically shown here, but confirmed by considering the pan-European trend of cloud number separately within different size bins: Smaller cloud bins indicated a negative trend, whereas for larger clouds the number increased over the years.

3.2 Interannual cloud fraction trends

In a final step, records of CF are derived by integrating the CSD according to Eq. 3. The contribution of clouds with horizontal scales from 30 m to 30 km (1 px to 1000 px) to the CF is henceforth referred to as "total" CF. This should not be associated with the real cloud cover, but the partial CF from clouds within the size range satisfying a power-law distribution. The actual CF was reduced not only by considering a limited range of cloud horizontal sizes, but also since all cloud fields outranging the Landsat footprint dimension (~ 200 km) are automatically neglected. The same applies for clouds touching the boundaries of the satellite scene. Moreover, Landsat T1 data precautionarily excludes heavily clouded scenes from the data set due to low quality conditions. Therefore, it can be assumed that in reality the CF was larger.

Fig. 6 shows the pan-European trend in the total CF over Europe (blue), and moreover, the individual contribution from different cloud size bins. The partial CF is derived as contribution from clouds with 30–300 m (1–10 px), 300–3000 m (10–100 px), and

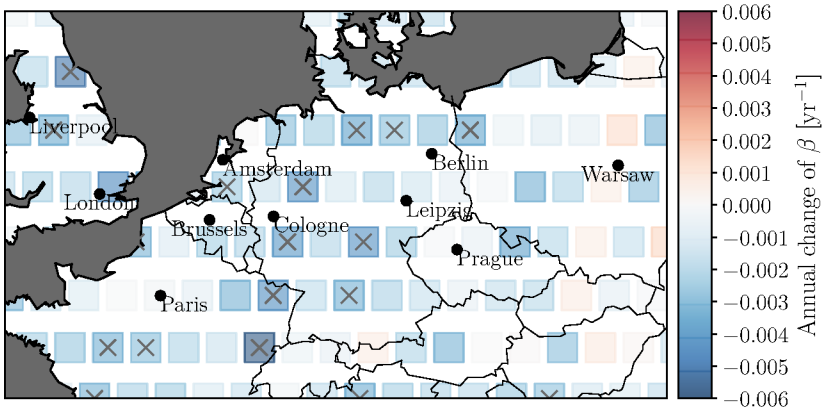

Figure 5: *Tile-specific trends of power-law exponent β during 1985–2018. Regions marked with cross indicate statistically significant trends with individual linear correlation coefficient $r > 0.4$, and RMSE $< \overline{RMSE}$. From a total of 143 Landsat tiles, 21 met the significance criteria, from which 17 are found on land and indicated within the map.*

3 km–30 km (100–1000 px) length, respectively, by correspondingly adjusting the limits of integration.

The total CF indicates an overall increase during 1985–2018 over Europe with 0.04 % per year accounting for the entire domain, and 0.15 % per year within the filtered data set. An increasing CF trend is further notable for the contribution from medium-sized and large clouds, but with decreasing significance towards smaller cloud sizes. For the smallest size bin, a slight reduction in the contribution to the CF is evident from the corresponding data. The contribution of partial CF to the total CF is dominated by large-scaled clouds. This is in agreement with our observed power-law exponent β: If the value of the exponent is below the scaling threshold 2, then large clouds dominate the CF, but with values larger than 2, small clouds contribute more to the overall CF (for more information see Wood and Field, 2011). Consequently, the overall trend in CF is also dominated by changes within larger cloud fields, due to $\beta < 2$.

By applying the statistical filter to the time series, each individual trend (partial and total CFs) is intensified and appears increasingly monotonic. However, from all 143 tiles only 9 (8, 6, 12) passed the thresholds to contribute to the filtered trend of total CF (partial CFs from 1–10, 10–100, 100–1000 px, respectively). The corresponding regions are marked in the map of Fig. 7, showing the spatial distribution of trends in total CF during the period 1985–2018.

Most grid-box trends show a widespread increase in CF over Europe. Grids with significant trends are exclusively positive, supporting the filtered time series that gives the average of these areas in panel (b) of Fig. 6. Some larger connected parts of Europe indicate negative trends, especially in eastern Germany extending towards the Czech Republic, and the Benelux, but with little statistical significance. Therefore, it can be concluded that there was a widespread increase in CF over Europe during 1985–2018.

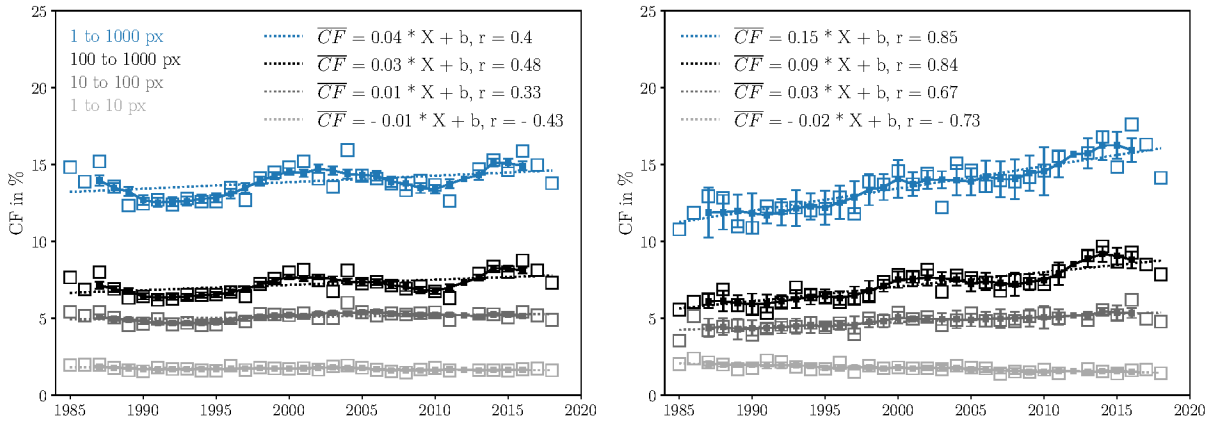

(a) (b)

Figure 6: *Pan-European trends in CF 1985–2018, (a) without filtering, and (b) after filtering for statistical significance, as raw data (larger empty squares), and low-frequency variability (5-yr moving average; filled smaller squares). The filtering excludes all Landsat footprints with trends r* < 0.4*, and RMSE* $> \overline{RMSE}$*. From the total of 143 tiles, 9 passed the filtering in the total CF (blue). Error bars give the standard error of mean, and a linear regression fit is used to derive the overall trend 1985–2018. CF trends were derived separately as contribution from clouds within different size ranges by correspondingly adjusting the limits of integration. All clouds with 30 m to 30 km (1–1000 px) length are contributing to the "total" CF.*

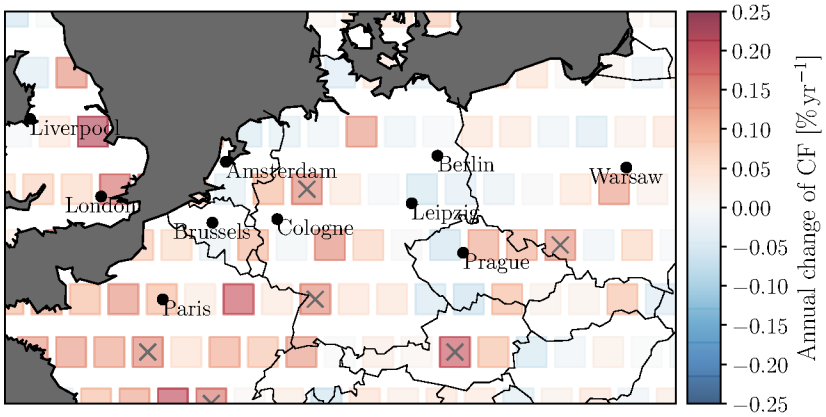

Figure 7: *Grid-box trends of total CF during 1985–2018. Regions marked with cross indicate statistically significant trends with individual linear correlation coefficient r* $>$ 0.4*, and RMSE* $< \overline{RMSE}$*. From a total of 143 Landsat tiles, 9 met the significance criteria, from which 6 are found on land and indicated within the map.*

4 Discussion

For deriving trends in cloudiness over Europe we adapt the method of Wood and Field (2011) to determine CSDs by cloud segment length. The primary result of deriving an overall CSD over Europe including the entire Landsat collection is the emergence of a power-law fit that spans over three orders of magnitude of cloud horizontal scales ranging from 30 m to 30 km. The quantification of the overall exponent with $\beta = 1.73$ is in good agreement with previous studies using observational data sets but also from numerical simulations (Guillaume et al., 2018). The power-law is further valid when breaking down the data set to account for regional and annual distributions. The tile-specific power-law exponent remained below the scaling threshold 2. This supports the common knowledge that the cloud cover is dominated by larger clouds, whereas the contribution to the number density increases towards smaller cloud sizes.

To circle back to the previously defined research question, our first attempt was to identify potential cloud changes in our data set of CSDs during past decades. The pan-European trend in the CSD indicates a large-scale decrease in the number of small clouds, together with an increase in the relative abundance of larger cloud fields of several 100 m length and more. The reduction/increase in the number of small/large clouds reflects in the corresponding trends of partial CFs. Overall, there was an increase in the total CF during 1985–2018 widespread over Europe, which becomes monotonic by filtering the entire data for robust trends among the grid boxes.

But are there trends real, and if so, can they be attributed to the European aerosol decrease since the late 1980s? The cloud record is in alignment with the findings of Norris and Wild (2007), who showed an overall dropping downward solar cloud-cover radiative effect due to an increasing CF during 1987–2002. They estimate the enhancement in cloudiness with $+0.9 \pm 1.7$ % per decade. The Landsat data set accounts for a CF trend of +0.4 % per decade within the unfiltered trend, and +1.5 % per decade for the filtered time-series, which matches the estimated range of Norris and Wild (2007).

Norris and Wild (2007) attribute the cloud record to natural weather and climate variability since a long-term increase in cloud cover occurred at the same time as aerosol concentrations decreased. However, this argumentation alone might not be enough to exclude a major impact of the European aerosol concentration decrease. Clouds can adjust through other processes than precipitation suppression. However, according to recent conclusions of Rosenfeld et al. (2019), the isolation of the pure aerosol effect most likely results in an overall positive correlation that is indeed mainly mediated by the aerosol effect on coalescence and precipitation.

Another point of interest is the role of cloud horizontal sizes in the cloud adjustments. Our hypothesis suggests that individual cloud-size classes might respond in a different manner to an aerosol perturbation: Smaller clouds are more exposed to entrainment drying due to their surface-to-volume ratio. However, our observational data suggests a decrease in the number of smaller clouds and the corresponding partial CF, even though aerosol loads have been dropping. The opposite is true for larger clouds, which would not be expected from a pure aerosol impact.

Rosenfeld et al. (2019) attribute negative aerosol-CF relationships from previous studies to an effect of local meteorology. The CF response appears to be strongly tied to atmospheric conditions (e.g., ambient relative humidity) that can obscure the actual

aerosol effect. But do local meteorological conditions reflect in our observed CF trend?

For individual cloud records among the grid boxes, the trends were mostly weak and of low statistical significance, so that the signal-to-noise ratio would justify the attribution to natural variability. Moreover, local minima within the cloud record fall together with noteworthy drought years, e.g., 2003, 2015, and 2018 (see again Fig. 6 (a) and (b), without low-frequency filter). Those drought events are mostly driven by precipitation deficits and rising temperatures (Hanel et al., 2018). This gives us another indication of a likely impact of local meteorology on the CF trend. Additionally, a negative aerosol-CF relationship has been found in several studies before, and was interpreted as effect of local meteorology and climate variations (Sato and Suzuki, 2019).

The remaining question is whether cloud changes are entirely explained by natural internal variability or whether they can be attributed to ACIs by further resolving the data set spatially and temporally. By mapping annual grid-box trends, some areas show a decrease in CF (e.g., Benelux regions, parts of Eastern Germany and Czech Republic). However, these trends are not significant and interpreting them within the context of ACIs is premature. It remains unclear what else impacts the cloud record and to what extent local trends are individually affected.

5 Summary and conclusions

In this study, we derive CSD and CF trends over Europe during 1985–2018, including satellite data from Landsat 5 to 8. During this time, the European aerosol burden experienced a large-scale decrease, which has likely led to a decrease in cloud albedo onward from the late 1980s (Krüger and Graßl, 2002; Norris and Wild, 2007). However, ACIs might have been additionally mediated by cloud adjustments concerning properties like the CF.

So far, scientists have not reached a consensus on the sign of the aerosol-CF relationship due to the coexistence of precipitation suppression (Albrecht, 1989), and evaporation feedbacks (Ackerman et al., 2004; Small et al., 2009) which might either increase, or decrease cloudiness through an increase in aerosol numbers. We use the CSD as observational link, derived from the Landsat-GEE data catalogue and computational routines. Due to its general spectral characteristics and long-term data record, Landsat data has the potential to carry out multidecadal cloud studies.

Our derived European CSD follows the expected power-law relation, and shows a larger relative abundance of small clouds over large clouds. The co-variation of slope and intercept of the power-law distribution further allows for the derivation of CFs from the represented clouds sizes. The observations indicate an increase within the pan-European CF during 1985–2018, thereby suggesting a negative relationship between aerosol amount and CF. However, considering the results of recent studies, the isolated aerosol-CF effect is more likely represented by a positive relationship (Gryspeerdt et al., 2016; Rosenfeld et al., 2019).

We still consider the change in CSD and CF a real trend. However, based on current knowledge it is more likely that other confounding factors contributed to the trend rather than the European aerosol reductions. We speculate on the impact of local meteorology and climate variability which can obscure the aerosol impact on clouds.

As articulated before, additional data (e.g., trends in temperature and precipitation) need to be considered within the chain of causality between aerosol amount and CF to isolate potential adjustments embedded in ACIs. More attention should be payed to robust trends indicated within individual cases, as they might outweigh both the effect of natural variability, and spurious trends from satellite retrieval anomalies. This topic is left as an outlook for subsequent studies.

Acknowledgements

We acknowledge the processing service Google Earth Engine for providing a platform for algorithm development which allowed us to preprocess and download high-resolution Landsat. The authors would like to thank Oliver Lahr for providing Fig. 1.

References

Ackerman, A. S., Kirkpatrick, M. P., Stevens, D. E., and Toon, O. B. (2004). The impact of humidity above stratiform clouds on indirect aerosol climate forcing. *Nature*, 432(7020):1014.

Albrecht, B. A. (1989). Aerosols, Cloud Microphysics, and Fractional Cloudiness. *Science*, 245(4923):1227–1230.

Boucher, O., Randall, D., Artaxo, P., Bretherton, C., Feingold, G., Forster, P., Kerminen, V.-M., Kondo, Y., Liao, H., Lohmann, U., et al. (2013). Clouds and aerosols. In *Climate change 2013: the physical science basis. Contribution of Working Group I to the Fifth Assessment Report of the Intergovernmental Panel on Climate Change*, pages 571–657. Cambridge University Press.

Cubasch, U., Wuebbles, D., Chen, D., Facchini, M., Frame, D., Mahowald, N., and Winther, J. (2013). Introduction. In *Climate change 2013: the physical science basis. Contribution of Working Group I to the Fifth Assessment Report of the Intergovernmental Panel on Climate Change*, pages 119–158. Cambridge University Press.

Gryspeerdt, E., Goren, T., Sourdeval, O., Quaas, J., Mülmenstädt, J., Dipu, S., Unglaub, C., Gettelman, A., and Christensen, M. (2018). Constraining the aerosol influence on cloud liquid water path. *Atmospheric Chemistry and Physics Discussions*, 2018:1–25.

Gryspeerdt, E., Quaas, J., and Bellouin, N. (2016). Constraining the aerosol influence on cloud fraction. *Journal of Geophysical Research: Atmospheres*, 121(7):3566–3583.

Guillaume, A., Kahn, B. H., Yue, Q., Fetzer, E. J., Wong, S., Manipon, G. J., Hua, H., and Wilson, B. D. (2018). Horizontal and Vertical Scaling of Cloud Geometry Inferred from CloudSat Data. *Journal of the Atmospheric Sciences*, 75(7):2187–2197.

Hanel, M., Rakovec, O., Markonis, Y., Máca, P., Samaniego, L., Kyselỳ, J., and Kumar, R. (2018). Revisiting the recent European droughts from a long-term perspective. *Scientific reports*, 8(1):1–11.

Jiang, H. and Feingold, G. (2006). Effect of aerosol on warm convective clouds: Aerosol-cloud-surface flux feedbacks in a new coupled large eddy model. *Journal of Geophysical Research: Atmospheres*, 111(D1).

Jiang, H., Xue, H., Teller, A., Feingold, G., and Levin, Z. (2006). Aerosol effects on the lifetime of shallow cumulus. *Geophysical Research Letters*, 33(14).

Krüger, O. and Graßl, H. (2002). The indirect aerosol effect over Europe. *Geophysical Research Letters*, 29(19):31–1–31–4.

Lohmann, U. and Feichter, J. (2005). Global indirect aerosol effects: a review. *Atmospheric Chemistry and Physics*, 5(3):715–737.

Norris, J. R. and Wild, M. (2007). Trends in aerosol radiative effects over Europe inferred from observed cloud cover, solar "dimming", and solar "brightening". *Journal of Geophysical Research: Atmospheres*, 112(D8).

Rosenfeld, D., Zhu, Y., Wang, M., Zheng, Y., Goren, T., and Yu, S. (2019). Aerosol-driven droplet concentrations dominate coverage and water of oceanic low-level clouds. *Science*, 363(6427):eaav0566.

Sato, Y. and Suzuki, K. (2019). How do aerosols affect cloudiness? *Science*, 363(6427):580–581.

Small, D. J., Chuang, P., Feingold, G., and Jiang, H. (2009). Can aerosol decrease cloud lifetime? *Geophysical Research Letters - GEOPHYS RES LETT*, 36.

Twomey, S. (1974). Pollution and the planetary albedo. *Atmospheric Environment (1967)*, 8(12):1251 – 1256.

Wood, R. and Field, P. R. (2011). The Distribution of Cloud Horizontal Sizes. *Journal of Climate*, 24(18):4800–4816.

Xue, H. and Feingold, G. (2006). Large-Eddy Simulations of Trade Wind Cumuli: Investigation of Aerosol Indirect Effects. *Journal of the Atmospheric Sciences*, 63(6):1605–1622.

Xue, H., Feingold, G., and Stevens, B. (2008). Aerosol Effects on Clouds, Precipitation, and the Organization of Shallow Cumulus Convection. *Journal of the Atmospheric Sciences*, 65(2):392–406.